



# Full-duplex enabled wireless power transfer system via textile for miniaturized IMD

Jaeho Lee<sup>1</sup> · Beomjun Bae<sup>2</sup> · Beomjin Kim<sup>2</sup> · Byunghun Lee<sup>1,2</sup>

Received: 12 April 2022 / Revised: 8 June 2022 / Accepted: 28 June 2022 / Published online: 17 July 2022  
© Korean Society of Medical and Biological Engineering 2022

## Abstract

Full-duplex (FD) enabled wireless power transfer (WPT) system via textile for miniaturized IMD is presented. By utilizing the battery-free near-field communication (NFC) method, the system realizes wireless power and data transmission without a bulky battery or energy harvester which can diminish the physical size of implantable medical device (IMD). Moreover, using textile as a medium of power transmission, the system overcomes the drawback and extends the limited effective range of the NFC method. In addition, as realizing simultaneous bidirectional data transmission over a single data channel, IMD has been further miniaturized. The proposed system including an external transmitter and the minimized IMD receiver supports 200 kbps and 50 kbps data rates for FSK downlink and LSK uplink telemetries at the same time with bit error rate (BER) of  $<8 \times 10^{-5}$  and  $<4 \times 10^{-5}$ , respectively. The measured power transfer efficiency (PTE) and DC-to-DC power delivered to load (PDL) are 5.77% and 64 mW at 0.5/60 cm of vertical/horizontal distance.

**Keywords** Full duplex · Wireless power transfer · Conductive thread · Textile coil · Data telemetry · Implantable medical device · Dual-band · Near-field-communication method · Radio frequency technology

## 1 Introduction

Implantable medical devices (IMDs) are electronic devices placed inside the human body for various purposes of continuous monitoring, diagnosis, and treatment [1–3]. As taking partial care of medical analysis and healthcare, the IMDs have improved the quality of human life by minimizing contact between patient and hospital which will be especially desirable in the future where diverse epidemics are predicted since the Covid-19 pandemic [4, 5]. Thus, demand on IMDs is rapidly increasing, which can easily be witnessed from the expected global IMD market value of 179,032 M\$ in 2030 [6]. With the ever-growing popularity, the IMDs are aggressively studied to develop. Since the IMDs are surgically inserted into the body and attached to biological tissue,

physical size is one of the most important design factors which may impair surrounding tissues or hinder the movement of patients [7–13].

A typical IMD system consisting of an external transmitter (Tx) and implanted receiver (Rx) requires bidirectional data communication by which Tx sends data (downlink) to control or adjust the Rx while the Rx transfers data of recorded biological information back to the Tx (uplink) [14]. In general, the two-way transmission is conducted over two communication channels or a single channel with additional complex circuitry (e.g. time-division multiplexing circuit) which eventually increases the physical size of the Rx [15]. Moreover, the recent IMDs utilize RF-based technology such as Bluetooth or Wi-Fi to enable distant wireless communication. However, such RF-based technology causes high power consumption, eventually enlarging the circuit area due to the bulky battery as well as the wireless communication module itself [16]. In addition, RF wireless communication also suffers from privacy and security issues due to vulnerability to eavesdropping, possibly bringing patients into fatal risk without the use of complex cryptography techniques [17, 18].

In this work, a full-duplex (FD) enabled wireless power transfer (WPT) system via textile for miniaturized IMDs

✉ Byunghun Lee  
blee22@hanyang.ac.kr

Jaeho Lee  
leejh6783@hanyang.ac.kr

<sup>1</sup> Department of Electronic Engineering, Hanyang University, Seoul 04763, South Korea

<sup>2</sup> Department of Biomedical Engineering, Hanyang University, Seoul 04763, South Korea

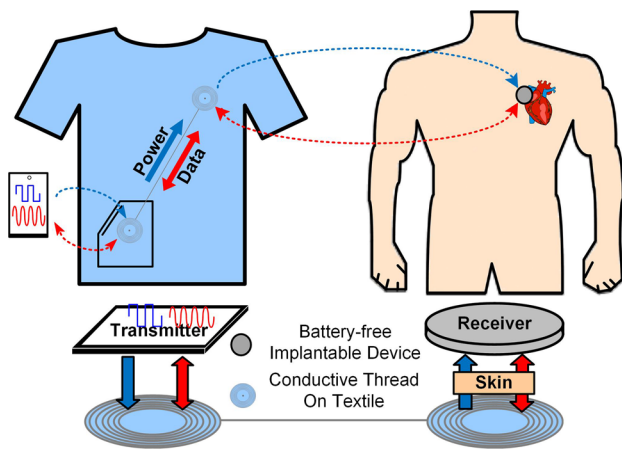


**Fig. 1** Illustration of wireless power and full duplex data transmission of implantable medical device system via textile

is presented. To realize bidirectional data transmission over a single channel without any complex circuitry, frequency shift-keying (FSK) and load shift-keying (LSK) are employed as downlink and uplink telemetries, respectively. Moreover, we utilize the battery-free near-field communication (NFC) method rather than RF wireless communication to overcome the aforementioned challenges. However, NFC wireless communication is available only when the Tx and Rx are placed very closely which is the major drawback of the NFC method. Hence, we utilize conductive thread embroidered on textile to extend the limited effective range of the NFC.

There have been several types of research that worked on the WPT system utilizing textile [19–29]. Heo et al. [19], Jiang et al. [20], Xu et al. [21], Escobedo et al. [22], Chang et al. [23, 26], Grabham et al. [24] and Sun et al. [25] analyzed detailed characteristics of textile and verified the feasibility of textile usage on the WPT system. However, they utilized textile as a driving coil so that rigid electronic elements of subsequent circuits have to be attached to the textile, which can possibly be damaged by dynamic movement or laundry process. On the other hand, the WPT system presented in [27–29] used textile as a medium of transferring power but they verified power transfer with on–off keying (OOK) on the LED without a specific data rate which can only support one-way data transmission. As illustrated in Fig. 1, the external Tx provides both power and data transmission to the battery-free Rx across textile while the Rx can also simultaneously send data back to the Tx even with a single communication channel. Unless the Tx escapes a certain distance from the textile, power, and data transmission are feasible at an arbitrary position near the body.

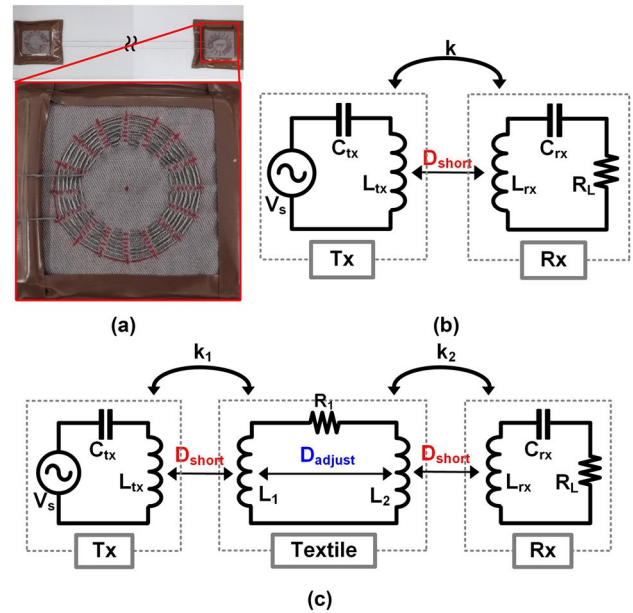


**Fig. 2** a Conductive thread embroidered on textile, circuit schematic of b typical NFC system and c textile-utilized NFC system

## 2 NFC range extension via textile

NFC-based devices have multiple advantages compared to RF-based devices. Among the various benefits, the most fundamental one is that the NFC-based devices can be battery-free whereas RF-based devices usually employ a bulky battery or energy harvester. Thus, RF-based devices are not favorable to biomedical or implantable devices due to their tight physical limitation. Although NFC-based devices are preferred for the above reason, they are hardly utilized in a variety of applications because of the short effective distance. NFC-based devices can function only within a few centimeters, and efficiency dramatically drops as the devices escape a certain distance from the Tx device. However, this challenge can be solved by the textile. Since the conductive thread can be regarded as a metal with high resistance, a coil-shaped thread embroidered on textile as shown in Fig. 2a can be seen as a low-Q inductor that is still able to induce the magnetic field. Thus, unlike the typical NFC-based system by which the Tx and Rx should be located at a short distance as illustrated in Fig. 2b, the in-between textile can be used as a medium of power transmission, eventually extending the transmission range by lengthening the in-between textile stage as shown in Fig. 2c. However, each textile coil should be closely located with the Tx and Rx to be inductively coupled. Considering that the Rx is a medical device implanted in a fixed location of the body whereas the Tx can be a smartphone in an IMD system, we assume that span-based daily cloth can also hold Tx at a specific position

(e.g. inside a shirt pocket). Then, embroidered textile coils on the two appointed spots could maintain a short distance from the Tx and Rx. To minimize power loss caused by the conductive thread, we chose low resistance DEV-13814 as the conductive textile which has  $27 \Omega/m$ .

### 3 Conventional FD data transmission

#### 3.1 FSK downlink telemetry

It is well known that FSK modulation has a variety of advantages compared to other modulation techniques. The FSK modulation not only has higher immunity to various distortions such as noise and other interference, but it is also easy to decode with simple circuit implementation [12]. However, conventional FSK that utilizes single resonant frequency suffers from narrow bandwidth, consequently decreasing power transfer efficiency (PTE) in a high-speed application. On the other hand, a dual-band FSK that utilizes two resonant frequencies can achieve high PTE at each resonant frequency [30]. As shown in Fig. 3a, the dual-band can be easily implemented with the serial connection of the LC-branch and the LC-tank in the Rx while an additional switch with a capacitor,  $C_{tx2}$ , is adopted on the Tx. This dual-band implementation realizes the FSK at two resonant frequencies,  $f_1$  and  $f_2$ , which satisfies

$$f_1 = \frac{1}{2\pi\sqrt{L_{tx1}(C_{tx1} + C_{tx2})}} = \frac{1}{2\pi\sqrt{(L_{rx1} + Z_{tank})C_{rx1}}}, \quad (1)$$

$$f_2 = \frac{1}{2\pi\sqrt{L_{tx1}C_{tx1}}} = \frac{1}{2\pi\sqrt{L_{rx1}(C_{rx1} \parallel Z_{tank})}}, \quad (2)$$

$$Z_{tank} = \begin{cases} j\frac{\omega L_{rx2}}{1-\omega^2 L_{rx2}C_{rx2}} = L_{tank} @f_1, \\ -j\frac{\omega L_{rx2}}{\omega^2 L_{rx2}C_{rx2}-1} = C_{tank}, @f_2. \end{cases} \quad (3)$$

According to (3), the LC-tank in Rx acts as the equivalent inductor,  $L_{tank}$ , in the lower frequency,  $f_1$ , and the equivalent capacitor,  $C_{tank}$ , in the higher frequency,  $f_2$ . In the Tx, the switch either attaches or detaches  $C_{tx2}$  by which two resonant frequencies are obtained at  $f_1$  and  $f_2$  based on (1) and (2). Hence, as illustrated in Fig. 3b, the dual-band implementation enables the FSK modulation with the high PTE at both frequencies.

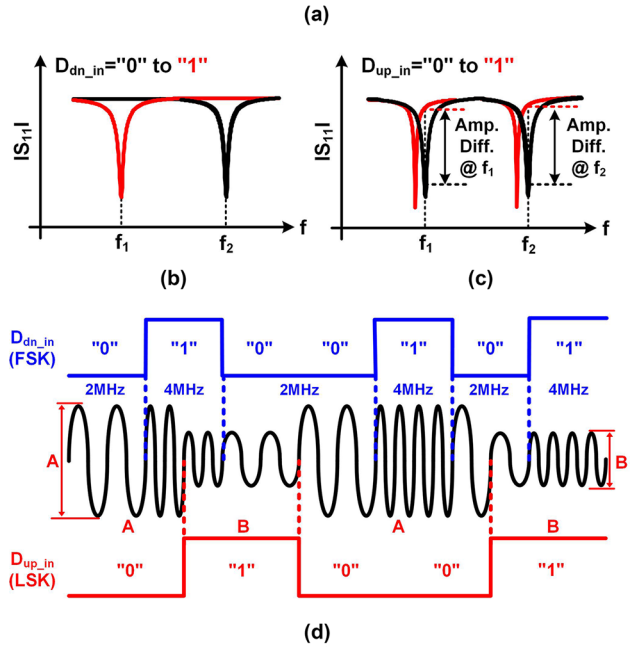
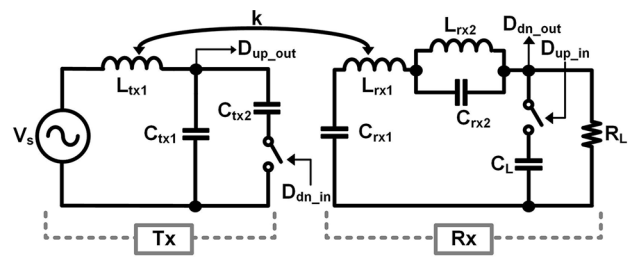


Fig. 3 a Circuit implementation of conventional FD transmission, concept of b FSK and c LSK, d conceptual overall waveforms

#### 3.2 LSK uplink telemetry

LSK modulation is typically used in the low-power or area-efficient applications because it can be easily implemented with a single switch without high power consumption. However, utilizing the LSK modulation as uplink telemetry with the conventional FSK downlink simultaneously is not feasible since it affects the frequency response of the received FSK signal. This issue is also solved by the dual-band module since the dual-band module provides a more robust transmission by which each carrier uses the resonant point of the respective band. Therefore, as shown in Fig. 3a, the LSK modulation is implemented in the Rx with a single switch and capacitor,  $C_L$ . When the switch is closed,  $C_L$  affects the system the resonant frequency which can be calculated as follows:

$$f_{reflected} = \frac{1}{2\pi\sqrt{(L_{tx1} + L_{reflected})C_{tx}}}, \quad (4)$$

$$L_{reflected} = j\omega^3 k^2 L_{tx1} L_{rx1} C_L, \tag{5}$$

$$\text{where } k = \frac{M}{\sqrt{L_x L_y}}$$

Based on (4) and (5), the reflected impedance from the  $C_L$  shifts down and dislocates the system resonant frequency. Due to the resonant frequency shift, the amplitude of the carrier signal seen on  $D_{up\_out}$  decreases at both  $f_1$  and  $f_2$  as shown in Fig. 3c. Therefore, LSK uplink and FSK downlink data can be decoded by the carrier amplitude and frequency difference at the same time. The conceptual overall waveform of the FD transmission is illustrated in Fig. 3d.

### 4 FD data transmission via textile

#### 4.1 FSK downlink telemetry

In order to enable longer-distance wireless power transmission through the NFC method, the textile is utilized between the Tx and Rx by which the Tx coil,  $L_{tx1}$ , and Rx coil,  $L_{rx1}$ , are inductively coupled with the textile coils,  $L_1$  and  $L_2$ , as shown in Fig. 4a. The in-between textile stage along with the Rx results in the reflected impedance which shifts the target resonant frequency although both the Tx and Rx are designed to precisely resonate at the target frequency. The reflection can be calculated as follows:

$$Z_{reflected} = \frac{\omega^2 k_1^2 L_1 L_{tx1}}{R_1 + j\omega(L_1 + L_2) + \frac{\omega^2 k_2^2 L_2 L_{rx1}}{R_L}}, \tag{6}$$

$$C_{reflected} = \frac{\left(R_1 + \frac{\omega^2 k_2^2 L_2 L_{rx1}}{R_L}\right)^2 + \omega^2(L_1 + L_2)^2}{\omega^4 k_1^2 L_1 L_{tx1} (L_1 + L_2)}, \tag{7}$$

$$f_{shifted} = \frac{1}{2\pi \sqrt{L_{tx}(C_{tx} \parallel C_{reflected})}}. \tag{8}$$

Based on (6)–(8), reflected reactance can be seen as the serially connected capacitor on the Tx side which reduces the overall capacitance of the Tx and consequently shifts up the system resonant frequency as shown in Fig. 4b. Therefore, we compensate for it by increasing both  $C_{tx1}$  and  $C_{tx2}$  based on (7) and (8) to improve the decreased PTE due to the effect of the textile stage.

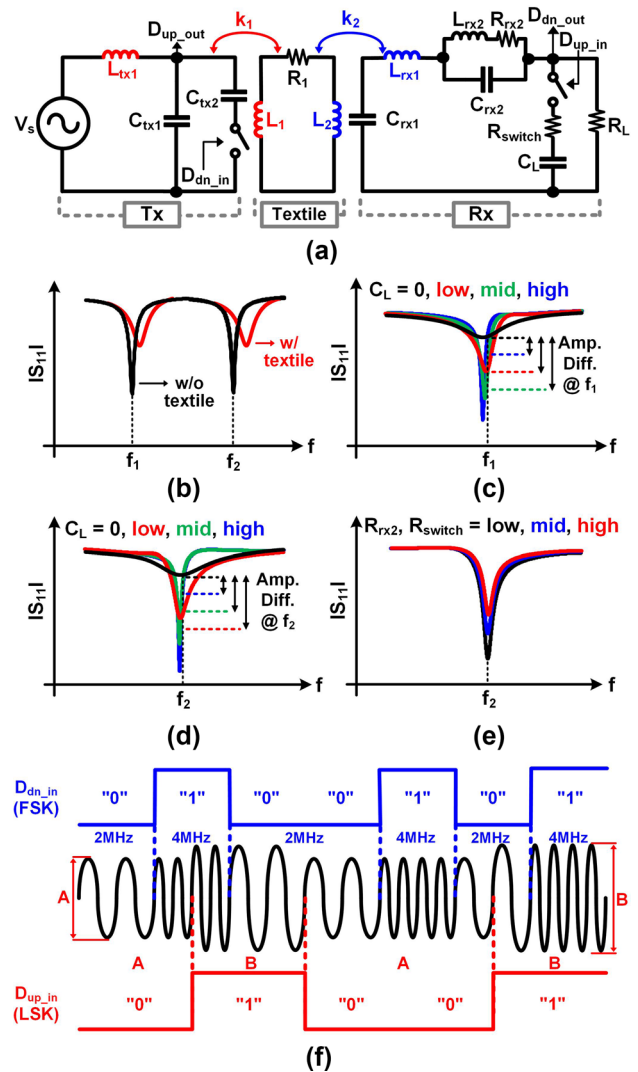


Fig. 4 a Circuit implementation of FD transmission via textile, concept of b FSK, and LSK c at  $f_1$ , d at  $f_2$ , e effect of  $R_{rx2}$  and  $R_{switch}$ , f conceptual overall waveform of the proposed system

#### 4.2 LSK uplink telemetry

The in-between textile stage also has influence on the effect of  $C_L$ . The influenced reflection can be calculated as follows:

$$C_{CL-on} = \frac{\omega^2(L_1 + L_2 + C_L \omega^2 k_2^2 L_2 L_{rx1})^2 + \left(\frac{\omega^2 k_2^2 L_2 L_{rx1}}{R_L} + R_1\right)^2}{\omega^4 k_1^2 L_1 L_{tx1} (L_1 + L_2 + C_L \omega^2 k_2^2 L_2 L_{rx1})^2} \tag{9}$$

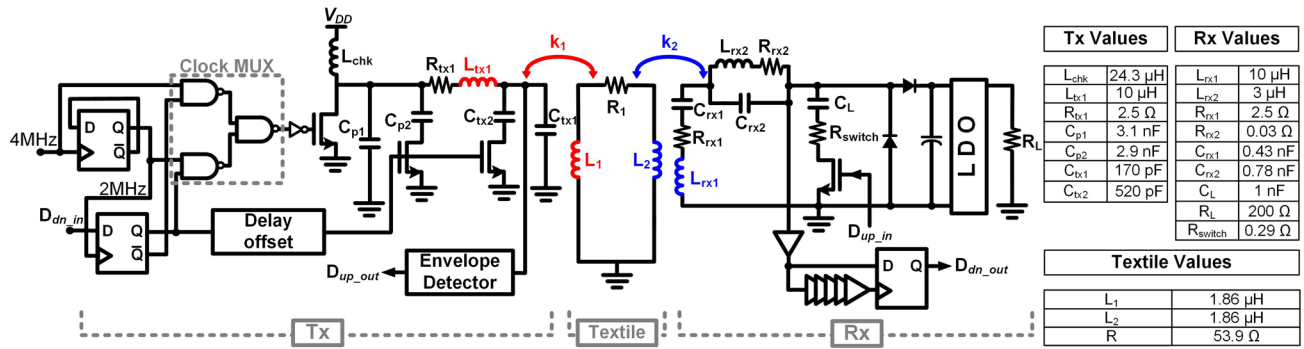


Fig. 5 Overall schematic and components values of the proposed system

$$R_{CL-off} = \frac{\frac{w^2 k_2^2 L_2 L_{rx1}}{R_L} + R_1}{w^2 (L_1 + L_2)^2 + \left(\frac{w^2 k_2^2 L_2 L_{rx1}}{R_L} + R_1\right)^2}, \tag{10}$$

$$R_{CL-on} = \frac{\frac{w^2 k_2^2 L_2 L_{rx1}}{R_L} + R_1}{w^2 (L_1 + L_2 + C_L w^2 k_2^2 L_2 L_{rx1})^2 + \left(\frac{w^2 k_2^2 L_2 L_{rx1}}{R_L} + R_1\right)^2}. \tag{11}$$

Based on (9), the reflected reactance when  $C_L$  is shorted can be seen as the serial capacitor,  $C_{CL-on}$ , in the perspective of the Tx. However, unlike  $L_{reflected}$  from (5),  $C_{CL-on}$  is not directly proportional to the capacitance of  $C_L$  which has less impact on shifting the resonant frequency. Furthermore, according to (10) and (11), the reflected resistance decreases when  $C_L$  is attached, eventually increasing the system quality factor. Therefore, attachment of  $C_L$  brings the increased amplitude of carrier signal while attachment of  $C_L$  in the conventional system without the textile stage dislocates the resonant frequency and brings the decreased amplitude at the target frequency. Since the LSK does not work as it does in the conventional system where  $C_L$  is simply selected if it is high enough to dislocate the resonant frequency, careful selection of  $C_L$  is required for the robust LSK transmission. Moreover, the proposed system utilizes the simultaneous dual-band FSK telemetry so that the LSK has to work in two frequencies. However, as illustrated in Fig. 4c, d, there is an optimal  $C_L$  at each frequency where maximum amplitude difference is achieved due to the frequency-dependent factor,  $w$ , from (9) and (11). Thus,  $C_L$  has to be selected considering the amplitude difference at both frequencies based on the (9)–(11). Nonetheless, compared to the conventional LSK, the amplitude difference is relatively smaller such that it may be susceptible to multiple variations and distortion. Hence, it is important to maximize the variation of reflected impedance on the Tx in order to enable more robust LSK transmission. Since minimized resistance

Table 1 Prototype inductive link specifications

Parameters	Value
Double layer printed spiral Tx and Rx coil ( $L_{tx1}$ and $L_{rx1}$ )	Inductance = 10 $\mu$ H Outer diameter = 3.5 cm Line width/spacing = 0.4/0.25 mm Number of turns = 7 $\times$ 2 Thickness = 1 oz Quality factor = 87
Textile coil	Inductance = 1.86 $\mu$ H Outer diameter = 3.5 cm Line width/spacing = 0.12/1 mm Number of turns = 7 $\times$ 1 Quality factor = 3
Vertical/horizontal distance	0.5/60 cm
Coupling coefficient	0.79
Carrier frequency ( $f_1, f_2$ )	2 MHz, 4 MHz
Loading ( $R_L$ )	200 $\Omega$

$R_{rx2}$  of  $L_{rx2}$  and  $R_{switch}$  of MOSFET switch can magnify the amplitude as shown in Fig. 4e, the selection of high-Q  $L_{rx2}$  and MOSFET switch with low on-resistance improves the robustness of LSK transmission. The conceptual overall waveform of the system is illustrated in Fig. 4f.

### 5 Measurement results

Figure 5 shows the overall schematic and components values of the proposed system. For frequency compensation due to the textile stage,  $C_{tx1}$  and  $C_{tx2}$  are selected with higher capacitance than the resonant capacitance at both 2 MHz and 4 MHz with  $L_{tx1}$ .  $C_L$  is carefully chosen to fairly differentiate the carrier amplitude at both frequencies. To further increase the amplitude difference on the Tx for the robust LSK transmission, NRS6028T3R0NMGJ is used for high-Q



**Fig. 6** Experimental setup of the proposed system

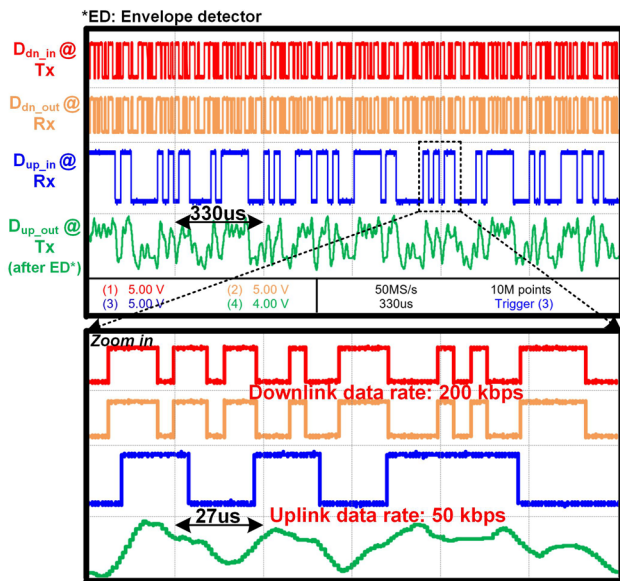
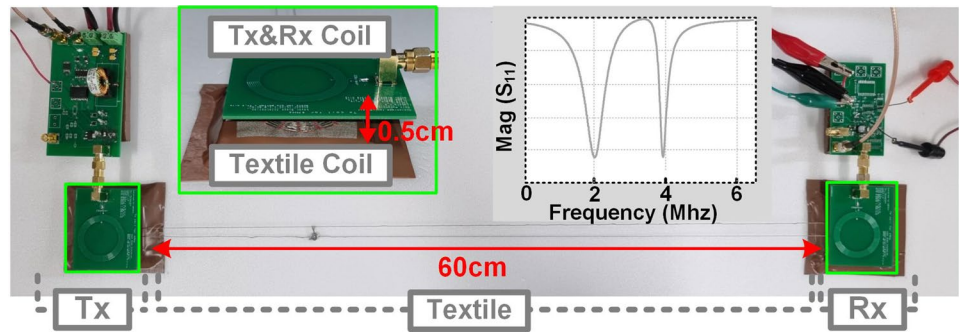


**Fig. 7** Measured transient waveforms of FD data transmission via textile coils

$L_{rx2}$ , and RSF015N06TL is employed for low on-resistance MOSFET switch. Overall specifications of Tx/Rx/textile coils are listed in Table 1. Specifications of textile coils are measured with the network analyzer (E5063A, Keysight).

Figure 6 demonstrates the experimental setup of the proposed system. The Tx/Rx coils are located 0.5 cm vertical distance from the textile coils while the horizontal distance between two textile coils is 60 cm. The coupling coefficient  $k_1$  and  $k_2$  are 0.79.

Since the measurement is conducted with a proof-of-concept prototype, the occupied area of the Rx board is  $2.4 \times 3.3 \text{ cm}^2$  with the Commercial Off-the-Shelf (COTS) devices excluding elements adopted only for test purpose, which can be further scaled down with ASIC design.

Figure 7 shows the measured transient waveforms of FD data transmission via textile. Date rate of LSK uplink and FSK downlink telemetries are 50 and 200 kbps, respectively. Considering the Tx has less limitation on area than the Rx, the LSK uplink data can be simply recovered through an envelope detector while the FSK downlink data are recovered through few area-efficient digital logic blocks. The

**Table 2** Comparison with previous works

	[15]	[31]	[32]	[33]	[34]	[35]	[36]	[37]	[38]	Proposed
Usage of textile	No	No	No	No	No	No	No	No	Yes	Yes
Full/half-duplex	Half	Half	N/A	Half	Half	Half	Full	Full	Half	Full
Frequency	27.1 MHz	275/131 MHz	2/4 MHz	0.022 MHz	60 MHz	2/0.125 MHz	1.2/2 MHz	2/4 MHz	N/A	2/4 MHz
Distance (V/H)*	0.4–1.4 cm	1.8 cm	0.6 cm	2.5 cm	0.5 cm	N/A	N/A	1 cm	N/A	0.5/60 cm
Coil diameter (Tx/Rx)	60/50 mm	25/2 mm	35/20 mm	165/165 mm	29/3.2 mm	40/20 mm	N/A	35/20 mm	125/125 mm	35/35 mm
Uplink mod	LSK	OOK	N/A	BFSK	ASK	BPSK	OOK	LSK	N/A	LSK
Downlink mod	ASK/BPSK	ASK	FSK	BFSK	OOK	BPSK	OOK	FSK	N/A	FSK
Uplink data rate	300 kbps	1 Mbps	N/A	120 bps	160	N/A	80kbps	14 kbps	60kbps	50 kbps
Downlink data rate	500 bps	N/A	1 Mbps	120 bps	50kbps	N/A	80kbps	800 kbps	60kbps	200 kbps
Uplink BER	$< 10^{-4}$	$2.7 \times 10^{-6}$	N/A	N/A	N/A	$< 10^{-7}$	N/A	$< 10^{-6}$	N/A	$4 \times 10^{-5}$
Downlink BER	$< 10^{-6}$	N/A	$< 10^{-5}$	N/A	N/A	$< 10^{-7}$	N/A	$3.12 \times 10^{-5}$	N/A	$8 \times 10^{-5}$
PDL	60 mW	0.11 mW	126 mW	700 W	2.7 mW	N/A	600 W	140 mW	50mW	64 mW
PTE (DC-to-DC)	–	2.01%	25%	85%	2.4%	N/A	N/A	14%	N/A	5.77%

\*V/H Vertical/horizontal distance

measured bit error rate (BER) of uplink and downlink telemetries are  $<4 \times 10^{-5}$  and  $<8 \times 10^{-5}$ , respectively. The proposed system wirelessly delivers 64mW power to the load while 5.77% DC-to-DC PTE is achieved through the two-coil inductive link along with the textile during simultaneous LSK and FSK modulations. Table 2 presents a comparison with prior works. Since most prior works using the textile coils in the WPT system only demonstrate the proof-of-concept design without either the data rate or PTE, the proposed work is compared with the previous works without textile coils, which report the BER and PTE.

## 6 Conclusion

This article presents the WPT system via textile which can not only diminish the physical size of IMD but also enable FD transmission with simultaneous FSK downlink and LSK uplink telemetries via textile. Through mathematical analysis and simulation results, this article has analyzed the effect of textile on the WPT system and has realized robust FD transmission at 2MHz and 4 MHz. With a simple circuit structure, minimized physical size, and a fairly high data rate with decent PTE, the proposed system can be applied to diverse IMDs as well as other low-power or battery-free wearable applications. To the best of our knowledge, the proposed work is the first fully implemented WPT system to succeed in FD data transmission via textile.

**Funding** This work was supported by the National Research Foundation of Korea (NRF) Grant funded by the Korea Government (No. 2021R1C1C1009986).

## Declarations

**Conflict of interest** The authors declare that they have no conflict of interest.

**Ethical approval** This article does not contain any studies with human participants or animals performed by any of the authors.

## References

- Lee SB, et al. An inductively powered scalable 32-ch wireless neural recording system-on-a-chip with power scheduling for neuroscience applications. *IEEE Trans Biomed Circuits Syst.* 2010;4(6):360–71.
- Kim C, et al. A 144 MHz fully integrated resonant regulating rectifier with hybrid pulse modulation for mm-sized implants. *IEEE J Solid-State Circuits.* 2017;52(11):3043–55.
- Lee H-M, et al. Stimulation efficiency with decaying exponential waveforms in a wirelessly-powered capacitive discharging stimulation system. *IEEE Trans Biomed Eng.* 2018;65(5):1095–106.
- Schwab JO, Wiese J, Hauser T. The influence of the 2020 COVID-19 pandemic on the implantation rates of cardiac implantable electronic devices in Germany: changes between 2020 Q1–Q3 and 2019 Q1–Q3. *Eur Heart J Qual Care Clin Outcomes.* 2022;8(2):104–12. <https://doi.org/10.1093/ehjqcco/qcab091> (PMID: 34849668; PMCID: PMC8690261).
- Maines M, Palmisano P, Del Greco M, Melissano D, De Bonis S, Baccillieri S, Zanotto G, D’Onofrio A, Ricci RP, De Ponti R, Boriani G. Impact of COVID-19 pandemic on remote monitoring of cardiac implantable electronic devices in Italy: results of a survey promoted by AIAC (Italian Association of Arrhythmology and Cardiac Pacing). *J Clin Med.* 2021;10(18):4086. <https://doi.org/10.3390/jcm10184086> (PMID: 34575197; PMCID: PMC8469719).
- Terdale S, Sumant O. Implantable medical devices market by product (orthopedic implants, cardiovascular implants, intraocular lens, dental implants, breast implants, other implants): global opportunity analysis and industry forecast, 2020–2030. Allied Market Research. 2022. <https://www.alliedmarketresearch.com/implantable-medical-devices-market>
- Medical Device and Diagnostic Industry. A one-size-fits-all approach can be dangerous for certain implantable medical devices. *Medical Device and Diagnostic Industry News.* 2015. <https://www.mddionline.com/why-size-matters-when-it-comes-medical-devices>
- Bazaka K, Jacob M. Implantable devices: issues and challenges. *Electronics* 2012;2(4):1–34. <https://doi.org/10.3390/electronics2010001>
- Lee HM, Ghovanloo M. Power-efficient wireless neural stimulating system design for implantable medical devices. *IEIE Trans Smart Process Comput.* 2015;4(3):133–40.
- Cho J, Seong G, Chang Y, Kim C. Energy-efficient integrated circuit solutions toward miniaturized closed-loop neural interface systems. *Front Neurosci.* 2021;15:667447. <https://doi.org/10.3389/fnins.2021.667447>
- Lee H-M, Park H, Ghovanloo M. A power-efficient wireless system with adaptive supply control for deep brain stimulation. *IEEE J Solid-State Circuits.* 2013;48(9):2203–16.
- Lee B, Lee H-M (2022) Wireless applications: biomedical signals telemetry system. In: Sawan M, editors. *Handbook of biochips: integrated circuits and systems for biology and medicine*, Ch. 44; Springer, 2022.
- Kim C, et al. A 3 mm × 3 mm fully integrated wireless power receiver and neural interface system-on-chip. *IEEE Trans Biomed Circuits Syst.* 2019;13(6):1736–46.
- Rosa BMG, Anastasova S, Yang GZ. NFC-powered implantable device for on-body parameters monitoring with secure data exchange link to a medical blockchain type of network. *IEEE Trans Cybern.* <https://doi.org/10.1109/TCYB.2021.3088711>
- Tang X, et al. A fully-integrated 27.12 MHz inductive power and data telemetry link for biomedical implants. In: *IEEE 63rd int. midwest symp. on circuits and systems*; 2020. p. 655–658.
- Gabrillo LJ, Galesand MG, Hora JA. Enhanced RF to DC converter with LC resonant circuit. In: *IOP conference series: materials science and engineering*, vol. 79. no. 1. IOP Publishing; 2015.
- Bandodkar AJ, Jeang WJ, Ghaffari R, Rogers JA. Wearable sensors for biochemical sweat analysis. *Annu Rev Anal Chem.* 2019;12:1–22.
- Kim J, Campbell AS, Avila B, Wang J. Wearable biosensors for healthcare monitoring. *Nat Biotechnol.* 2019;37:389–406.
- Heo E, Choi KY, Kim J, Park JH, Lee H. A wearable textile antenna for wireless power transfer by magnetic resonance. *Text Res J.* 2018;88(8):913–21.
- Jiang Y, et al. Smart textile integrated wireless powered near field communication body temperature and sweat sensing system. *IEEE J Electromagn, RF Microwaves Med Biol.* 2019;4(3):164–70.

21. Xu L, et al. Characterization and modeling of embroidered NFC coil antennas for wearable applications. *IEEE Sens J.* 2020;20(23):14501–13.
22. Escobedo P, et al. The effect of bending on laser-cut electro-textile inductors and capacitors attached on denim as wearable structures. *Text Res J.* 2020;90(21–22):2355–66.
23. Chang C-W, Riehl P, Lin J. Embroidered coils—integration of wireless charging receiver coils in smart garments. *IEEE Int Symp Radio-Freq Integr Technol (RFIT).* 2021;2021:1–3.
24. Grabham NJ, Li Y, Clare LR, Stark BH, Beeby SP. Fabrication techniques for manufacturing flexible coils on textiles for inductive power transfer. *IEEE Sens J.* 2018;18(6):2599–606.
25. Sun D, Chen M, Podilchak S, et al. Investigating flexible textile-based coils for wireless charging wearable electronics. *J Ind Text.* 2020;50(3):333–45.
26. Chang C-W, Riehl P, Lin J. Embroidered textile coils for wireless charging of smart garments. *IEEE Wirel Power Transf Confer (WPTC).* 2021;2021:1–4.
27. Garnier B, et al. Textile NFC antenna for power and data transmission across clothes. *Smart Mater Struct.* 2020;29(8):085017.
28. Kim H-J, Lin R, Achavananthadith S, Ho JS. Near-field-enabled clothing for wearable wireless power transfer. *IEEE Wirel Power Transf Confer (WPTC).* 2020;2020:22–5.
29. Lin R, et al. Wireless battery-free body sensor networks using near-field-enabled clothing. *Nat Commun.* 2020;11(1):1–10.
30. Kung M-L, Lin K-H. Enhanced analysis and design method of dual-band coil module for near-field wireless power transfer systems. *IEEE Trans Microw Theory Tech.* 2015;63(3):821–32. <https://doi.org/10.1109/TMTT.2015.2398415>.
31. Yeon P, et al. Feasibility study on active back telemetry and power transmission through an inductive link for millimeter-sized biomedical implants. *IEEE Trans Biomed Circuits Syst.* 2017;11(6):1366–76.
32. Ahmadi MM. A class-E power amplifier with wideband FSK modulation for inductive power and data transmission to medical implants. *IEEE Sens J.* 2018;18(17):7242–52.
33. Lee K, Cho D. Maximizing the capacity of magnetic induction communication for embedded sensor networks in strongly and loosely coupled regions. *IEEE Trans Magn.* 2013;49(9):5055–62.
34. Lee B, et al. A triple-loop inductive power transmission system for biomedical applications. *IEEE Trans Biomed Circuits Syst.* 2015;10:138–48.
35. Gong C, Liu D, Miao Z, Wang W, Li M. An NFC on two-coil WPT link for implantable biomedical sensors under ultra-weak coupling. *Sensors.* 2017;17(6):1358. <https://doi.org/10.3390/s17061358>
36. Fan Y, Sun Y, Dai X, Zuo Z, You A. Simultaneous wireless power transfer and full-duplex communication with a single coupling interface. *IEEE Trans Power Elect.* 2021;36(6):6313–22. <https://doi.org/10.1109/TPEL.2020.3035782>.
37. Jung H, Lee B. Wireless power and bidirectional data transfer system for IoT and mobile devices. *IEEE Trans Indust Elect.* 2022;69(11):11832–6. <https://doi.org/10.1109/TIE.2021.3123609>
38. Catrysse M, Hermans B, Puers R. An inductive power system with integrated bi-directional data-transmission *Sens Actuators. A.* 2004;115(2-3):221–9.

**Publisher's Note** Springer Nature remains neutral with regard to jurisdictional claims in published maps and institutional affiliations.